Res Chem Intermed (2016) 42:2461–2471
DOI 10.1007/s11164-015-2161-8

Photocatalytic decolorization of reactive red 198 dye by a TiO_2–activated carbon nano-composite derived from the sol–gel method

Ameneh Eshaghi[1] · Sam Hayeripour[1] · Akbar Eshaghi[2]

Received: 22 April 2015 / Accepted: 1 July 2015 / Published online: 7 July 2015

Abstract In this research, a TiO_2–activated carbon nano-composite was prepared by a sol–gel method and characterized by XRD, FE-SEM, EDS, FTIR, BET surface area, photoluminescence spectroscopy and UV–Vis diffuse reflectance spectroscopy. The photocatalytic activity of the nano-composite was evaluated through degradation of reactive red 198 (RR 198) under UV light, and was compared to unsupported TiO_2. The XRD result indicated that the TiO_2 nano-composite contained only anatase phase. The surface area of the TiO_2 increased from 48 to 100 m^2/g through the fabrication of the nano-composite. The photocatalytic results indicated that the RR 198 was decolorized around 42 and 38 % during a 210-min irradiation period in the presence of nano-composite and TiO_2, respectively. It means that nano-composite enhanced the photocatalytic activity of the TiO_2 nanoparticles. After 20 h of irradiation in the presence of the nano-composite, 97 % of RR 198 had degraded.

Keywords TiO_2 · Nano-composite · Photocatalytic · Reactive red 198

Introduction

In recent years, concerns about steadily increasing water pollution due to the rapid growth of various industries and the high amount of wastewater generated have increased. It is well known that a significant amount of water is used for the dyeing

✉ Ameneh Eshaghi
paaeshaghi@gmail.com

[1] Faculty of Environmental Science, Tonekabon Branch, Islamic Azad University, Tonekabon, Iran

[2] Faculty of Materials Science and Engineering, Maleke Ashtar University of Technology, Isfahan, Shahinshahr, Iran

and finishing of fabrics in the textile industry [1, 2]. Therefore, the textile industry is one of the major producers of large volumes of toxic effluents, including synthetic dyes. These dyes, because of their toxicity and endurance, are hazardous to the environment. And, even when they are present in very low concentrations, they can have serious carcinogenic effects [3]. Because of this, the degradation of dyes in textile effluents has received increasing attention and several methods have been used. Traditional physical and chemical techniques, such as adsorption on activated carbon, ultrafiltration, reverse osmosis, coagulation by chemical agents, ion exchange on synthetic adsorbent resins, etc., have been used for the removal of dye pollutants. These techniques can, however, only transfer the contaminants (dyes) from one phase to another, thus generating secondary pollution. In addition, conventional biological treatment methods are ineffective for decolorization and degradation because of the high stability of theses dyes [4]. Consequently, traditional treatment methods are usually ineffectual at removing the dye. Hence, attention must be focused on treatment methods that can lead to the complete degradation of the dye molecules. Recently, advanced oxidation processes based on a semiconductor metal oxide photocatalyst have been effectively used for the decolorization and degradation of dyes in textile effluent [5–7]. Among semiconductor metal oxides, TiO_2 is one of the most promising nano-crystalline materials used as a photocatalyst in the degradation of organic pollutants due to its low cost, chemical stability, corrosion resistivity, and non-toxicity [8]. A TiO_2 photocatalyst has several advantages in organic pollutant degradation in comparison to traditional methods including (1) complete organic pollutant mineralization, (2) no waste solids generation, and (3) operation under mild temperatures and pressure conditions [9].

However, there are two drawbacks in using TiO_2 nano-particles during the photocatalytic process: (1) separation of the TiO_2 nano-particles from the treated wastewater is difficult, and (2) the suspended TiO_2 nano-particles tend to aggregate at high concentrations. So, in order to overcome these problems, much attention has been paid to immobilization of the TiO_2 nano-particles on support materials. In this respect, various types of supports for TiO_2 have been used including clay, zeolite, silica, perlite and activated carbon [10]. Among them, activated carbon (AC) has been used extensively as a support for heterogeneous catalysts. It has been reported that an AC-TiO_2 mixture has a positive effect on photocatalytic activity in the degradation of organic pollutants. In other words, AC, due to its high adsorption capability, can aid in enriching the organic pollutant around the TiO_2 nano-particles, increasing the pollution transfer process and, hence, promoting photocatalytic efficiency [11–18].

Liu et al. [19] investigated the photocatalytic degradation of phenol and methyl orange in the presence of a TiO_2–X wt% AC composite. They confirmed that the TiO_2–5 wt% AC composite showed the highest photoreactivity. In this research, TiO_2–5 wt% activated carbon nano-composite was prepared. Then, the photocatalytic activity of the nano-composite in the degradation of RR 198 dye was investigated.

Experimental

Fabrication of TiO_2–AC nano-composite

First, a TiO_2 precursor sol was prepared as following:

Tetrabutyl orthotitanate (5 mL, 97 %, Sigma Aldrich) was dissolved in absolute ethanol (50 mL) to form solution A, and a mixture of deionized water (250 mL) and H_2SO_4 (0.33 mL) was obtained as solution B. Solution B was then added to solution A dropwise while stirring. Then, TiO_2 sol was prepared. For the synthesis of the TiO_2–AC nano-composite, 0.06 g AC (AppliChem), which was prewashed with boiling water, was added slowly to the TiO_2 sol under vigorous stirring to avoid the formation of larger AC agglomerates in the sol. After magnetic stirring for 2 h, the mixture was kept in a water bath at 80 °C for 2 h. Finally, the mixture was cooled to room temperature, centrifuged, and washed with deionized water [12]. The as-obtained nano-composite was dried at 100 °C and then calcinated at 600 °C in an argon atmosphere. For comparison, TiO_2 nano-particles were synthesized by the same procedure without the addition of AC.

Characterization

The structure of the nano-composite was determined using a Bruker X-ray diffractometer (XRD, D8ADVANCE, Germany, Ni-filter, Cu Kα radiation $\lambda = 1.5406$ Å). The surface morphology and chemical composition of the nano-composite was measured by field emission scanning electron microscopy (FE-SEM, Hitachi S4160, cold field emission, voltage 20 kV) and energy-dispersive X-ray spectroscopy (EDS). The specific surface area of the nano-composite was evaluated using the Brunauer–Emmett–Teller (BET) method. The BET surface area was determined by nitrogen adsorption–desorption isotherm measurement at 77 K. The sample was degassed at 150 °C prior to actual measurement.

An UV–Vis spectrophotometer (Avantes, Avaspec-2048-TEC) was used to record the diffuse reflectance spectra of TiO_2 and TiO_2–AC nano-composite. BaSO4 was used as a reflectance standard in the UV–Vis diffuse reflectance experiment. Excitation and emission spectra of the samples were recorded by a photoluminescence (PL) spectrophotometer (Avantes, Avaspec-2048-TEC) using a xenon lamp as an excitation source operating at 355 nm.

The photocatalytic activities of the nano-composite under irradiation were evaluated by the decolorization rate of RR 198 (Dystar). RR 198 is one of the most representative and commonly used dyes in the textile industry [20]. In a typical experiment, 1 g/L of catalyst (nano-composite or TiO_2) was added to 100 mg/L of RR 198 solution while stirring. Then, the solution was irradiated with UV light (2 lamps, 15 W each, wavelength 254 nm). Before turning on the lamps, the dispersion was stirred in a dark place for 1 h, and during the photoreaction, solution samples were taken for analysis at regular intervals. The light absorbance of the RR 198 solution was measured using a UV–Vis spectrophotometer at 518 nm, which is the maximum absorption of RR 198 [20]. Then, the decolorization rate of the RR 198

was used to quantify the photocatalytic activities of the catalyst, and calculated using the following equation: [8]

$$\eta = \frac{A_0 - A}{A_0} \times 100 \quad (1)$$

where A_0 is the light absorbance of the RR 198 before the irradiation and A is the light absorbance of the RR 198 after the irradiation.

Results and discussion

Figure 1 shows the XRD patterns of the TiO_2 and TiO_2–AC nano-composite. The characteristic diffraction peaks of anatase at 25.4, 38, 48, 54.7, 63.1 were observed and no rutile peaks were detected. Therefore, the XRD measurements showed that both TiO_2 and the nano-composite contain only the anatase phase [10, 21, 22]. No other impurity phase could be detected.

Figure 2 shows the FE-SEM images of the TiO_2 and TiO_2–AC nano-composite. According to Fig. 2a, it can be seen that the average particle size of the TiO_2 is 35 nm. It is obvious that the AC has a clean and porous surface (Fig. 2b). Figure 2c shows that the TiO_2 nano-particles were well dispersed and loaded on the AC surface.

Energy dispersive X-ray (EDX) analysis was carried out to identify elements present on the nano-composite. The EDX spectrum of the surface of the nano-composite is illustrated in Fig. 3. Figure 3 shows the presence of carbon, titanium and oxygen in the nano-composite.

The transmission spectra of the samples were measured in the range of 4000–400 cm^{-1}, with a resolution of 4 cm^{-1}. Figure 4 shows the FTIR spectra of the samples. The adsorption band, at about 3400 cm^{-1}, is assigned to the stretching vibration of the O–H bonds and is related to surface-absorbed water. The adsorption band at 1600 cm^{-1} is attributed to the bending vibration of the H–O–H bonds, which is assigned to the chemisorbed water. The adsorption band at about 450 cm^{-1}

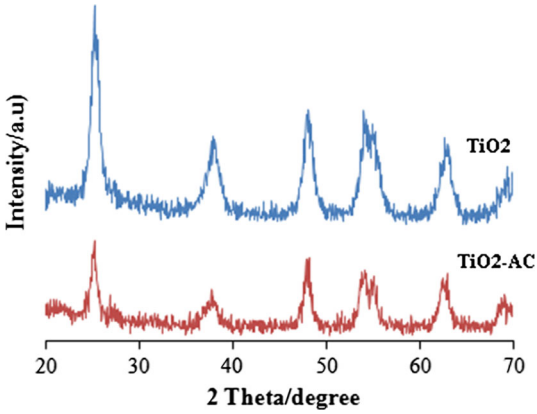

Fig. 1 XRD patterns of the TiO_2 and TiO_2–AC nano-composite

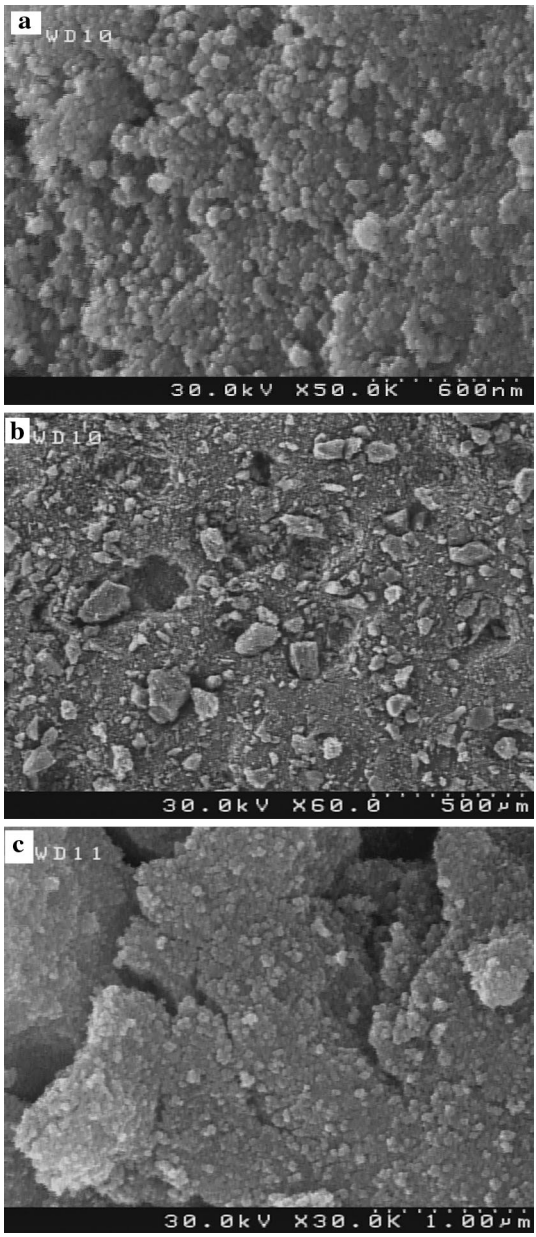

Fig. 2 FE-SEM images of **a** TiO2, **b** AC and **c** nano-composite

is due to the stretching vibrations of the Ti–O bonds [8]. However, with the addition of AC, a new peak was included at 1060 cm^{-1}. The adsorption band at about 1060 cm^{-1} may be ascribed to Ti–O–C, indicating a slight connection effect between bulk AC and Ti–O bonds [19]. It means the TiO_2 nano-particles attached

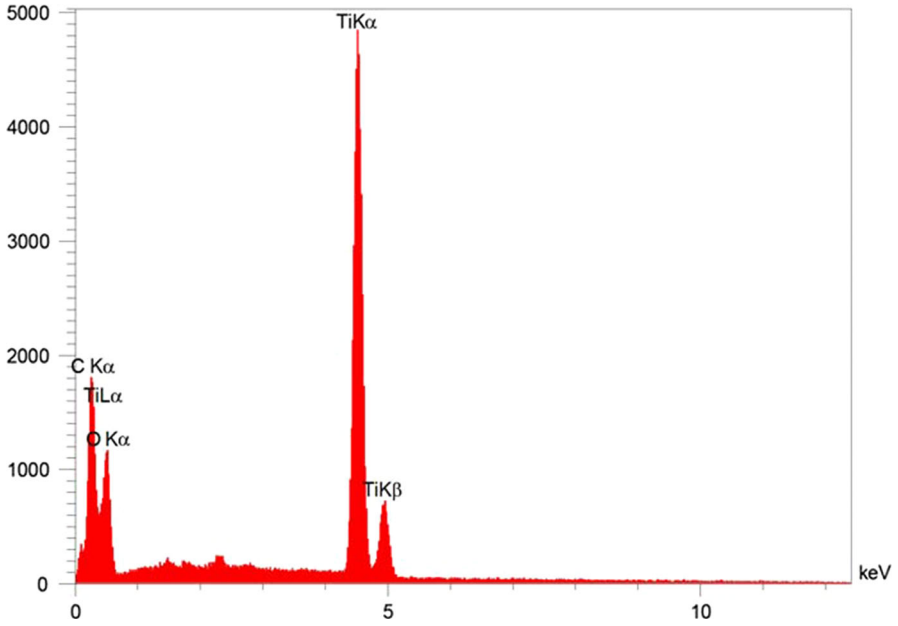

Fig. 3 EDAX spectrum of the TiO_2–AC nano-composite

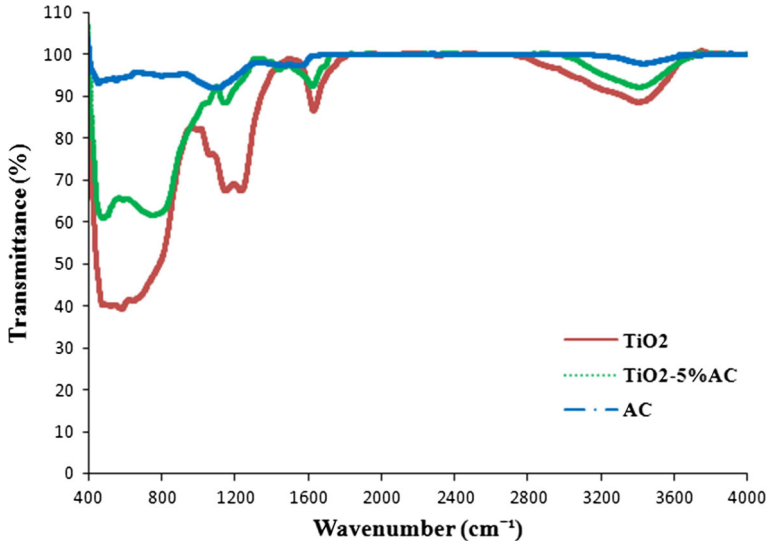

Fig. 4 FTIR spectra of the TiO_2, AC and TiO_2–AC nano-composite

chemically to the AC surfaces and are not easily separated. Therefore, concern about the separation and filtration of the TiO_2 nano-particles after wastewater treatment was resolved.

One of the main factors affecting photocatalytic performance is the surface area of the photocatalyst. Increasing the surface area is an effective method for increasing photocatalytic activity. Table 1 shows the BET surface area results of the samples. According to Table 1, it is clear that surface area of the TiO_2 increased from 48 to 100 m^2/g through the fabrication of the nano-composite. Therefore, AC exhibits a positive influence on catalyst surface area and, therefore, photocatalytic activity, which will be discussed in the following.

Figure 5 shows the diffuse reflectance spectra of the samples. It can be seen that TiO_2–AC nano-composite absorbs either in the UV and visible region in comparison to TiO_2. In other words, AC incorporation extended the absorption edge into the visible region and the catalyst absorbed stronger than pure TiO_2 in the 400–800 nm range, which may be due to the black characteristic of the AC [19].

PL emission spectroscopy has been widely applied to investigate the transition behavior of the photogenerated carriers, electrons and holes in semiconductor materials. It means that it can reflect the photogenerated electrons—holes separation and recombination in the semiconductor materials. The measured PL emission spectra of TiO_2 and TiO_2–AC nano-composite are illustrated in Fig. 6. The intensity of the PL spectra decreased for the TiO_2–AC nano-composite. This result shows that the PL intensity reduction indicates the decrease of the electron–hole pairs recombination process. Generally, a lower PL intensity indicates a lower photogenerated electron–hole pair recombination rate, which leads to higher photocatalytic activity [23].

Figure 7 shows the photocatalytic performance of the TiO_2 and TiO_2–AC nano-composite after 210 min of irradiation. Obviously, the photocatalytic efficiency of the TiO_2–AC nano-composite is higher than that of the TiO_2.

After 20 h of irradiation, the decolorization of the RR 198 in the presence of nano-composite and TiO_2 was measured around 95 and 85 %, respectively. Within 20 h, nearly complete removal of the RR 198 (97 %) could be achieved with the TiO_2-nano-composite. The decolorization images of the RR 198 at various intervals in the presence of the TiO_2–AC nano-composite are shown in Fig. 8.

The experimental results confirmed that the TiO_2 loaded on the AC adsorbent had greater photocatalytic efficiency for RR 198 decolorization than the unsupported TiO_2 , which we discuss in the following.

The photocatalytic mechanism of TiO_2 has been discussed generally in the literature [24–28]. When a TiO_2 photocatalyst is exposed to UV irradiation, with light energy greater than its band gap energy (3.2 eV), an electron and hole can be generated in the conduction and valence bands, respectively. The high oxidation potential of the holes (+2.6 V) can oxidize water or hydroxide to generate hydroxyl radicals. The hydroxyl radical is a strong oxidizing agent which leads to the partial

Table 1 BET surface area of samples

Sample	Surface area (m^2/g)
TiO_2	48.187
TiO_2–AC	100.337
AC	829.643

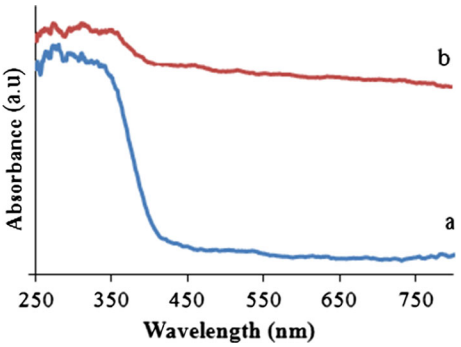

Fig. 5 Diffuse reflectance spectra of the (*a*) TiO_2 and (*b*) TiO_2–AC nano-composite

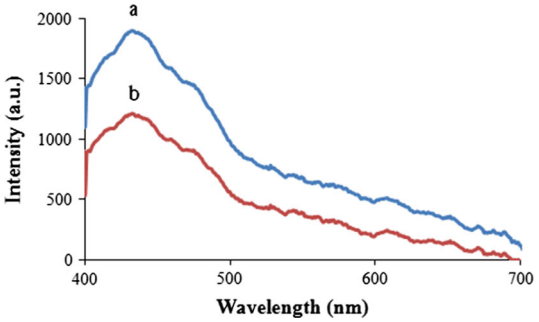

Fig. 6 PL spectra of the (*a*) TiO_2 and (*b*) TiO_2–AC nano-composite

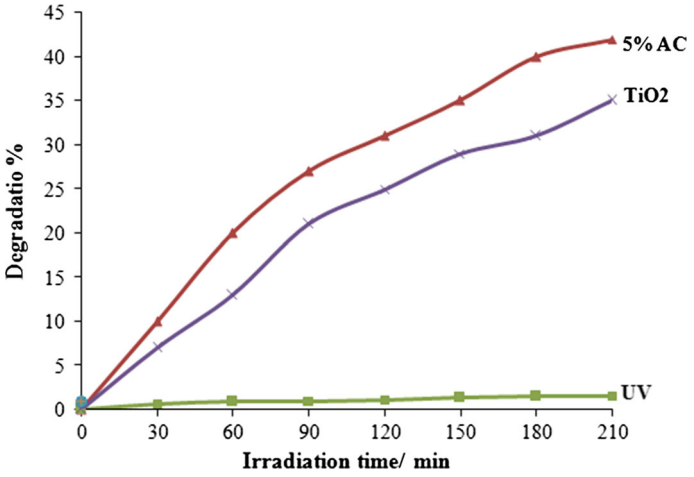

Fig. 7 Photocatalytic degradation of RR 198 after 210 min of irradiation

or complete mineralization of the RR 198 molecules. Then, the final products of the RR 198 molecules are H_2O, CO_2 and inorganic anions, including SO_4^{2-}, NO_3^- and Cl^-. The photo-generated electrons in the TiO_2 conduction band can reduce the

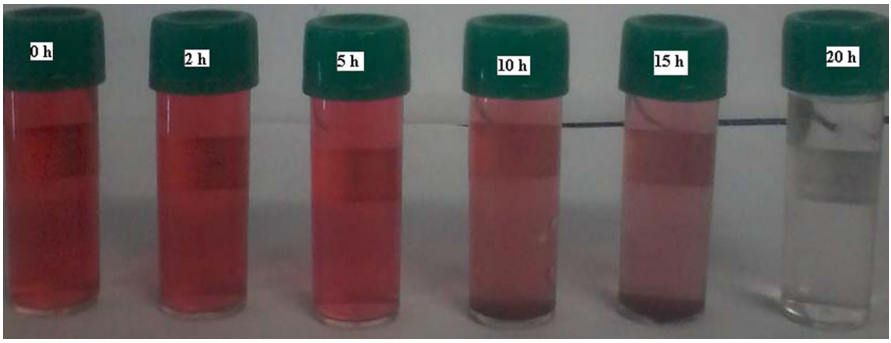

Fig. 8 Photocatalytic decolorization images of the RR 198 after various intervals of irradiation in the presence of TiO_2–AC nano-composite

oxygen molecule to superoxide anions. These superoxide anions are responsible for the production of the hydroxyl radicals that have been identified as the essential origin of RR 198 destruction [29, 30]. The whole photocatalytic mechanism of TiO_2 is summarized in Fig. 9.

As indicated in Fig. 7, AC enhanced the photocatalytic activity of the TiO_2. This enhancement can be attributed to the large adsorption capacity of the AC. AC is a highly porous solid carbon material with a very large surface area and high adsorption capacity. It provides large amounts of active adsorption sites; thus, the RR 198 molecules were adsorbed before transferring to the destruction center of the TiO_2. It is well known that an important step in the photocatalytic process is the adsorption of organic pollutants onto the surface of the catalyst. So, in the nano-composite, the RR concentration around the TiO_2 was higher than in the case of TiO_2 nano-particles only. Generally speaking, in the chemical reaction, the higher concentration leads to a faster reaction rate. Therefore, the nano-composite exhibited better photocatalytic performance than TiO_2 nano-particles. During the destruction process, the AC attracted and concentrated the RR molecules near the supported TiO_2 nano-particles. This would increase the reaction between the RR

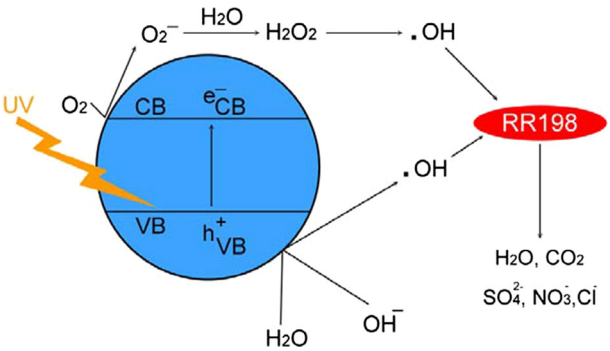

Fig. 9 General photocatalytic mechanism of the TiO_2 under UV irradiation

198 molecules and the hydroxyl radicals produced on the surface of the photoexited TiO_2, resulting in the enhanced RR degradation rate. In addition, during the fabrication of the nano-composite, AC was used to disperse the deposited TiO_2 nano-particles (Fig. 3c), inhibiting their agglomeration and, thus, increasing their photoreactivity under UV irradiation. During RR destruction near the surface of the nano-composite, the remainder of the RR 198 from the bulk solution would continue to be transferred and adsorbed by the nano-composite. In summary, it is concluded that the adsorption–photocatalysis synergistic process was responsible for the enhanced RR 198 removal rate with the nano-composite in comparison to the unsupported TiO_2 [9, 22]. The presumed mechanism for the photocatalytic decolorization of the RR 198 the with nano-composite is indicated in Fig. 10.

Conclusions

We reported the fabrication and photocatalytic investigation of TiO_2–activated carbon nano-composite. It was found that the photocatalytic activity of TiO_2 was improved by the addition of activated carbon. In fact, activated carbon not only increased the surface area of the catalyst and adsorption capacity but it also retarded the electron/hole pairs recombination process. Generally, a lower recombination

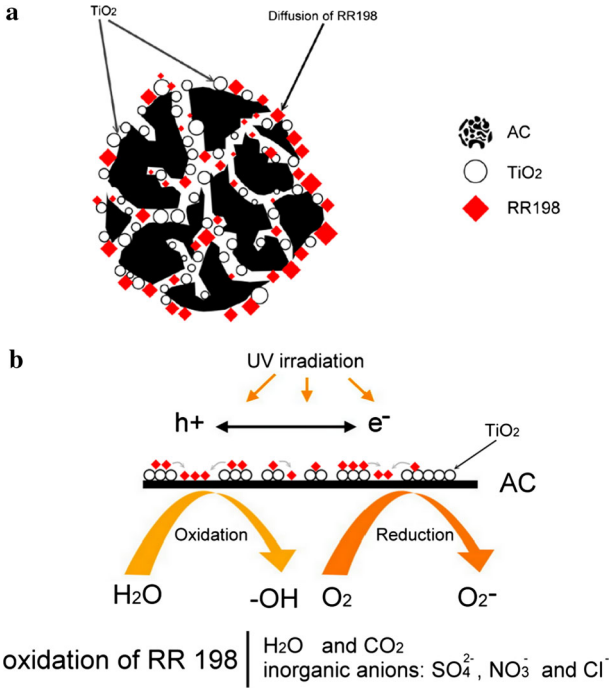

Fig. 10 Schematic illustrations of the RR 198 decolorization by TiO_2–AC nano-composite, **a** adsorption and **b** destruction

rate of photogenerated electron–hole pairs leads to greater photocatalytic activity of the photocatalyst.

References

1. K. Kaur, V. Singh, J. Hazard. Mater. **141**, 230 (2007)
2. C. Nasw, K. Vinodgopal, S. Hotchandanf, A. Kvinodgopal, A.K. Chattopadhyay, P.V. Kamat, Res. Chem. Intermed. **23**, 219 (1997). **KAMAT**
3. Y. Zhiyong, D. Bahnemann, R. Dillert, S. Lin, L. Liqin, J. Mol. Catal. A Chem. **365**, 1 (2012)
4. J. Sun, X. Yan, K. Lv, S. Sun, K. Deng, D. Du, J. Mol. Catal. A Chem. **367**, 31 (2013)
5. A. Saffar-Teluri, S. Bolouk, M.H. Amini, Res. Chem. Intermed. **39**, 3345 (2013)
6. D. Zhang, F. Zeng, Res. Chem. Intermed. **36**, 1055 (2010)
7. U.G. Akpan, B.H. Hameed, J. Hazard. Mater. **170**, 520 (2009)
8. A. Eshaghi, M. Pakshir, R. Mozaffarinia, Bull. Mater. Sci. **33**, 365 (2010)
9. N. Mohammad Mahmoodi, M. Arami, J. Zhang, J. Alloys Compd. **509**, 4754 (2011)
10. M. Asilturk, S. Sener, Chem. Eng. J. **180**, 354 (2012)
11. M. Hakamizadeh, S. Afshar, A. Tadjarodi, R. Khajavian, M.R. Fadaie, B. Bozorgi, Int. J. Hydrogen Energy **39**, 7262 (2014)
12. B. Gao, P.S. Yap, T.M. Lim, T.T. Lim, Chem. Eng. J. **171**, 1098 (2011)
13. A.K. Subramani, K. Byrappa, G.N. Kumaraswamy, H.B. Ravikumar, C. Ranganathaiah, K.M. Lokanatha Rai, S. Ananda, M. Yoshimura, Mater. Lett. **61**, 4828 (2007)
14. M.Q. Yang, N. Zhang, M. Pagliaro, Y.J. Xu, Chem. Soc. Rev. **43**, 8240 (2014)
15. Y. Zhang, Z.R. Tang, X. Fu, Y.J. Xu, ACS Nano **4**(12), 7303 (2010)
16. N. Zhang, Y. Zhang, Y.J. Xu, Nanoscale **4**, 5792 (2012)
17. C. Han, M.Q. Yang, B. Weng, Y.J. Xu, Phys. Chem. Chem. Phys. **16**, 16891 (2014)
18. A.E. Eliyas, L. Ljutzkanov, I.D. Stambolova, V.N. Blaskov, S.V. Vassilev, E.N. Razkazova-Velkova, D.R. Mehandjiev, Cent. Eur. J. Chem. **11**, 464 (2013)
19. S.X. Liu, X.Y. Chen, X. Chen, J. Hazard. Mater. **143**, 257 (2007)
20. N. Mohammad Mahmoodi, M. Arami, N. Yousefi Limaee, J. Hazard. Mater. **133**, 113 (2006)
21. L. Ravichandran, K. Selvam, M. Swaminathan, J. Mol. Catal A Chem. **317**, 89 (2010)
22. X. Wang, Y. Liu, Z. Hu, Y. Chen, W. Liu, G. Zhao, J. Hazard. Mater. **169**, 1061 (2009)
23. C.H. Kim, B.H. Kim, K.S. Yang, TiO_2 nanoparticles loaded on grapheme/carbon composite nanofibers by electrospining for increased photocatalysis. Carbon **50**, 2472–2481 (2012)
24. M.H. Baek, J.W. Yoon, J.S. Hong, J.K. Suh, Appl. Catal. A Gen. **450**, 222 (2013)
25. M.A. Rauf, S. Salman Ashraf, Chem. Eng. J. **151**, 10 (2009)
26. I. Konstantinou, T.A. Albanis, Appl. Catal. B Environ. **49**, 1 (2004)
27. S. Yao, J. Li, Z. Shi, Particuology **8**, 272 (2010)
28. A. Eshaghi, R. Mozaffarinia, M. Pakshir, A. Eshaghi, Ceram. Int. **37**, 327 (2011)
29. K. Naeem, F. Ouyang, J. Environ. Sci. **25**, 399 (2013)
30. J. Chen, C.S. Poon, Build. Environ. **44**, 1899 (2009)